

Curvature driven relaxation of disclination loops in liquid crystals

Janelle Gunther^a, Edwin L. Thomas^{a,*}, Scott Clingman^b and Christopher K. Ober^b

^a*Department of Materials Science and Engineering, Massachusetts Institute of Technology, 77 Massachusetts Ave., Cambridge, MA 02139, USA*

^b*Department of Materials Science and Engineering, Cornell University, Bard Hall, Ithaca, NY 14850, USA*

(Received 17 July 1997; revised 1 October 1997; accepted 22 October 1997)

Relaxation of disclination loops created during shear flow of a low molar mass and a polymer liquid crystal were monitored using a special shear stage with a videomicroscope. Loops in the polymer system generally displayed initially highly distorted contours. In the small molecule liquid crystal, the loop contours consistently exhibited very simple, generally convex shapes. In the polymer system, the complex line shape reflects the many prior loop–loop coalescence events due to the greater density of loops than in the small molecule system. Sequential images of loops were analysed to determine the velocity of the disclination loops as a function of the local curvature. Observations and simulations indicate that local disclination line curvature is a driving force in loop evolution. The reduction of regions of high loop curvature is inherently slower in the polymer liquid crystal due to the higher viscosity. In addition, the motion of the disclination contour at very high values of curvature in the polymer liquid crystal is slowed due to the presence of lower molecular weight components at the defect core which themselves must diffuse along with the line defect. © 1998 Elsevier Science Ltd. All rights reserved.

(Keywords: polymer liquid crystals; disclination loops; curvature flow)

INTRODUCTION

The motion of surfaces and interfaces is a common research theme throughout the physical sciences. An understanding of how surfaces and interfaces evolve over time can yield important information on relationships between structure, properties and materials processing conditions¹. The speed with which a line or surface moves can be described in a very general sense by a speed function, which is a function of local, global and independent properties². Independent properties are those that do not depend on the shape of the front. Fluid velocity would be one example. Global properties such as diffusion effects are those that depend on shape and position. Local properties are curvature and the direction of the normal.

Determining an expression for the speed function is a complex problem that has been addressed extensively in the literature in many different subject areas. Particularly active areas of research have been the study of crystal growth^{3–5} and evolution of grain boundaries in metals^{6–8}. These systems are affected by both local properties, such as curvature, and global properties such as solute diffusion. A study of the influence of curvature on grain boundaries in metals yielded important information on how impurities, strains, and boundary density affected the mode of motion of these surface defects. Similar work has also been carried out on line defects such as dislocations. Understanding the nature of the defect dynamics is a key component of structure–property relationships.

Line-like defects in liquid crystal systems have been considered theoretically by deGennes⁹. Simplifying

assumptions such as the equiconstant approximation ($k_{11} = k_{22} = k_{33}$) lead to an analytical solution for the distortions around a ‘disclination line’. The defect is modeled as a flexible string with an associated line tension, T , defined as the incremental increase in stored elastic energy per incremental increase in contour length. The energy per unit length associated with these disclination lines has the following form:

$$T = \int_a^{\rho_{\max}} 2\pi\rho \frac{1}{2} K \frac{s^2}{\rho^2} d\rho = \pi K s^2 \ln\left(\frac{\rho_{\max}}{a}\right)$$

where a is a lower limit of molecular dimensions (which defines the core region of the defect) and ρ_{\max} is an upper limit defined by the disclination spacing or by the distance between the disclination and a surface. For a disclination separation distance of 10 μm and a core size of about 10 \AA , the line tension is on the order of a few K (an elastic constant).

The line tension is a force that acts tangential to the disclination line. Minimization of line energy causes a disclination loop to shrink and eventually disappear. Disclination loop motion can be affected by a variety of forces. These include: line tension, forces between nearby portions of the loop or other defects, drag forces of the viscous fluid and diffusional effects associated with the segregation of impurities into the core. In addition, segregation of low molecular weight components in a polydisperse polymer system can lead to an additional force that further lowers the mobility. Finally, when the distance between opposite loop segments is very small, the interaction force begins to become significant. This can result in loop pinch-off events.

* To whom correspondence should be addressed

For an isolated loop, when the loop size is large (and the velocity relatively low), curvature driven motion (i.e. minimization of the line tension) is opposed by the viscous drag force^{10,11}. Assuming the line tension is approximately constant and neglecting other factors, a circular loop of radius R will shrink due to the interplay of line tension and the viscous drag force as:

$$R(t) = (t_0 - t)^{1/2}$$

In mathematics, the Grayson theorem states¹²: 'Any simple closed curve (i.e. non self-intersecting) moving under its curvature must shrink to a round point regardless of its initial shape.' This suggests that it may be possible to describe disclination loop evolution using mathematical algorithms that simulate curvature driven motion. A study of loop velocity *versus* loop curvature may give insight into the nature of disclination line tension and how it affects the shape and evolution of contours in both small molecule and polymer liquid crystals. This would also be of interest with respect to the evolution of defect walls created by applied magnetic fields. For example, Ding¹³ has noted that curvature smoothing of inversion walls is evident in their shrinkage and coalescence. That study focused on the formation mechanisms of Néel bend and Néel splay walls and their interaction dynamics. Calculations of wall energy as a function of elastic anisotropy was also examined. It was concluded that splay walls have a higher velocity than bend walls due to the higher energy of the former for the particular polymer liquid crystal under study. Although energy differences must have played a role in the dynamics, it is also possible that the effects could have been due to curvature variations as well.

The current paper reports an approach for studying curvature driven motion of disclination loops in liquid crystals. The motivation for this work is to understand the mechanisms by which disclination loops evolve during relaxation after shear flow. Graziano and Mackley were the first to investigate relaxation of disclinations after cessation of shear^{14,15}. They studied disclination loops in a low molar mass liquid crystal as well as in a thermotropic liquid crystalline polymer. Many other observations on the creation of and relaxation of disclinations have been reported, usually focusing on the variation of disclination density with shear rate and annealing time after cessation of shear, or after the isotropic to nematic transition^{10,11,16,17}.

EXPERIMENTAL

Synthesis and characterization of materials

The low molar mass liquid crystal 4-N-octyl-4'-cyano-biphenyl (8CB from BDH, Inc.) was used as received. This molecule has a smectic to nematic transition at 30°C and a nematic to isotropic transition at 42°C. The polymer DHMS-7,9 (with a mesogenic group of dihydroxymethylstilbene) with a number average molecular weight $M_n = 12\,000$ g/mol and weight average molecular weight $M_w = 25\,000$ g/mol was also used. The polymerization of the semi-rigid rod polymer was carried out using liquid/liquid phase transfer catalyzed polyetherification chemistry. An organic phase was used to dissolve the electrophilic monomers and polymer while a strong aqueous alkaline phase was used to dissolve the nucleophilic monomers¹⁸. The polymerization conditions allowed the synthesis of high molecular weight polyethers without strict control of stoichiometry. The best results were obtained when the

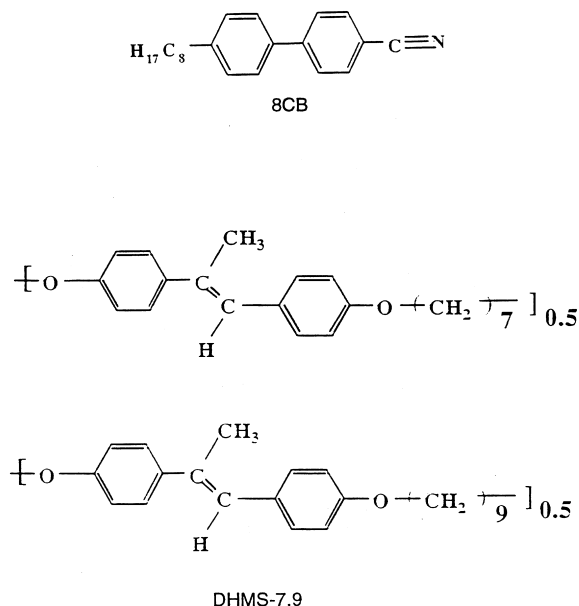


Figure 1 (a) The chemical structure of 8CB. (b) The chemical structure of DHMS-7,9

polymerizations were carried out with a 15% excess of the mesogen, DHMS, and a 1:1 molar ratio of the two flexible, aliphatic monomers. The procedure is described in detail elsewhere¹⁹. The chemical structures of both 8CB and DHMS-7,9 are shown in *Figure 1*.

Shear flow experiments

A new type of flow visualization apparatus known as an optical shearing apparatus, or shear cell, was used in this work. This machine was developed by Dr M. Mackley of Cambridge University, U.K. in conjunction with Linkham Scientific Instruments, Ltd.²⁰. This machine fits onto an optical microscope and enables *in situ* visualization of microstructural responses to shear from room temperature to 450°C. The sample is placed between two quartz windows which are in close thermal contact with a silver block heater. The plate separation is set by an electronic calibration procedure which is accurate to within $\pm 5\ \mu\text{m}$. The upper window is stationary while the bottom one is attached to a motor which rotates it according to the user-specified shearing conditions*.

For the experiments involving 8CB, the sample was loaded into the shear cell while the plates were slightly above the nematic to isotropic transition temperature. The gap was then set to a value of 100 μm . This value is large enough to minimize the error due to a $\pm 5\ \mu\text{m}$ variation in the gap setting, but also small enough for sufficient transparency. The sample was annealed in the isotropic state for approximately 5 min to erase the sample history. Next, the sample was cooled to 38°C. No disclination loops were seen initially. In order to generate these within the sample, a program of steady shear at 10 s^{-1} was used. The

* A careful cleaning procedure is followed to help ensure that the gap calibration will be as precise as possible. First, the quartz windows are soaked in an appropriate solvent (chloroform in this case) in order to remove excess polymer. Then the windows are subsequently rinsed with a sequence of ethanol and dish soap/water. This cycle is repeated until all residue is removed. If some residue remains even after 3 cycles, the windows are left in a bath of KOH and ethanol overnight. Following this treatment, the windows would then be subjected to one cycle of the above cleaning procedure.

resulting defect texture that appeared within a few minutes consisted of long disclination threads as well as disclination loops of various sizes. Both 'thicks' ($s = \pm 1$) and 'thins' ($s = \pm \frac{1}{2}$) defects were observed¹⁷. Our measurements were on $s = \pm \frac{1}{2}$ loops. In general, these defects were very gently curved. Whenever an entire disclination loop entered the field of view, the flow was stopped so that the loop relaxation process could be followed. Frames of interest were selected and digitized at a later time.

The experiments involving DHMS-7,9 were handled in a different way. Since the samples with the most readily observable textures were only available in small quantities (i.e. < 10 mg) a more simple setup was used to view the disclination loops. The sample was placed on a precleaned coverslip that was heated above the nematic to isotropic transition temperature. Another coverslip was then placed on top of the polymer to create a sandwich assembly. The sample was then annealed for 10 min in the isotropic state following which the sample temperature was lowered to 150°C. Upon reaching this temperature, many disclination loops were evident. Additional disclination loops were created by holding the bottom coverslip in place and oscillating the top coverslip back and forth. The shear rate was estimated at 10 s^{-1} . A DAGE-MTI CCD 72 camera and video recorder were used to follow the disclination behaviour in real time. By varying focus, we selected approximately planar loops for our study.

Curvature driven motion simulations

The study of curvature driven motion has been significantly aided by advances in mathematical analysis, particularly differential geometry. Several algorithms have been developed to study curvature motion. The earliest ones develop a differential equation to describe the motion of a particular curve and determine the form of the rate of change of boundary length as a function of time. More advanced methods use either marker or level set methods in order to follow the shape evolution of a space curve.

The type of algorithm most commonly used at present is a level set method. This was originally developed by Osher and Sethian²¹. Instead of following the motion of a set of markers, the algorithm tracks the motion of a plane curve. The original curve is incorporated into a surface that is designed so that it intersects the xy plane at the exact location of that curve. Instead of moving the original curve, the entire cone-shaped surface is manipulated. To determine how the curve changes over time, the cone-shaped surface is translated in the z direction to produce a new cross-section in the xy plane. The advantage of this method is that complex topological evolution (for example, when loops pinch off or when two loops coalesce) can be evaluated relatively easily without having to introduce correction algorithms during the process (as is the case with marker methods). Several computer codes are available that allow this type of modelling to be performed. The 'Surface Evolver', developed by Dr K. Brakke, is one such program²².

Curvature measurement algorithms

The approach of Allen and Rondeau²³ was used as the basis of the curvature measurement algorithms. Digitized images were used exclusively in this work to eliminate errors due to shifting and rotation of scanned images. These effects lead to scatter in the data which will be discussed in more detail in the following section. All micrographs were given as input to the NIH-Image software program. The point selection tool was used to extract the xy coordinates of

the disclination contours. The data files were ultimately used as input to a Matlab script file that reconstructed specific segments of the disclination contours. A series of curve fitting routines were then used to determine the order of the polynomial that best fit each set of data points. Comparisons were then made between pairs of curves, one of which was selected as a reference. The parameters supplied by the curve fitting routines were used to calculate the first and second derivatives for a given curve. A series of points on the original curve were selected for the curvature-velocity analysis. The equation of the local normal is then computed for the disclination curve at time t and the point where this line intersects the disclination curve at $t + \Delta t$ is then found. This information enables us to calculate the curvature at the corresponding location on the second equation for the disclination contour. The average local curvature was calculated as an arithmetic mean of the curvatures uniformly sampled along each individual curve. The local velocity was calculated by determining the displacement of the second curve with respect to the reference curve and then dividing by the corresponding time step, Δt .

RESULTS AND DISCUSSION

Disclination loop evolution

Two test problems we designed in order to evaluate the efficacy of the curvature measurement algorithms. In the first test problem a velocity *versus* curvature relationship was determined for a large circle shrinking to a smaller one. Since the curvature does not vary around the perimeter of a circle, the curvature for a given circle should remain constant. As a result, a plot of velocity *versus* curvature should yield a single straight line for a series of shrinking circles sampled at equal time intervals. For this particular test problem there are no errors associated with contour digitization, image registration or material flow. In practice, one must be very careful concerning image registration as well as to check for any material flow occurring between images.

Simulations of loop evolution were also used to test the theoretical model. A second test problem involved

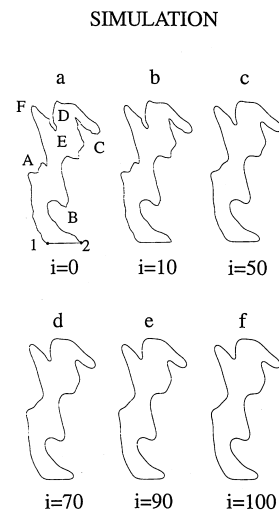


Figure 2 (a) A digitized image of a disclination loop in DHMS-7,9. The portion of the loop shown was artificially closed by connecting the points labeled '1' and '2'. (b)–(f) A sequence of simulations, produced with the Surface Evolver, that show how the original loop should evolve when the local curvature is the only driving force. The label 'i' indicates the number of program iterations that were performed. The additional labels 'A' to 'F' indicate regions of the simulations that show distinct changes throughout the series

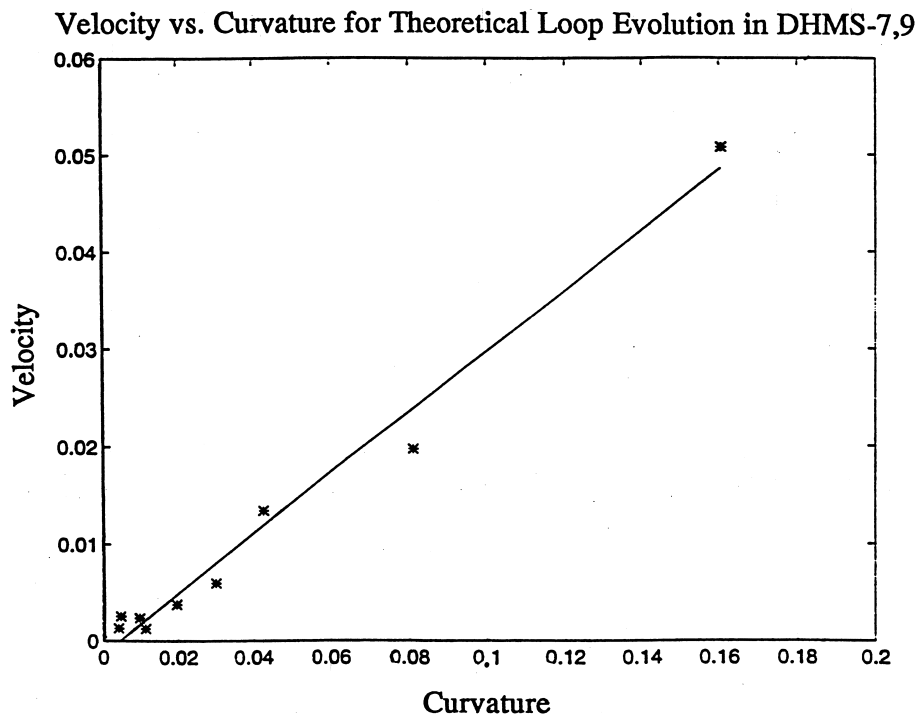


Figure 3 A plot of velocity *versus* curvature for the theoretical loop evolution using an actual disclination loop from DHMS-7,9 as the initial input (Figure 2a). The data fits a straight line well, indicating that the curvature measurement algorithm can yield results that are expected from mathematical theories

the application of the Surface Evolver program to model the evolution of a complex disclination curve using an actual experimental image for the initial input. A digitized image of a portion of the original loop is shown in Figure 2a. This was artificially allowed to be a closed loop by connecting the top of the loop (points 1 and 2). In the original image, these points constituted a part of the loop which extended beyond the viewing area. A sequence of images (Figure 2b–f) were then calculated with Surface Evolver to show how the loop should evolve theoretically over time when the local curvature is the only driving force. As expected, the regions of high curvature in the original image (e.g. feature A) become smoother in a short period of time while the regions of low curvature evolve more slowly (e.g. feature B). This was confirmed by velocity *versus* curvature measurements that were made on these simulations as well as additional iterations that are not shown. The results shown in Figure 3 fit a straight line remarkably well, again indicating that the algorithm is yielding reliable results.

Additional labels in the simulations (features C–F in Figure 2) indicate other regions of the disclination contour which show distinct changes throughout the simulations. In addition, the theoretically evolving contours can be directly compared with a time sequence of tracings obtained from experimental micrographs of the actual disclination. The original disclination loop is shown in Figure 4a. The subsequent tracings in Figure 4b–d show how the loop evolves after shear relaxation. Several interesting regions are indicated by the labels ‘A’ to ‘F’. These correspond to the identical labels in the simulations of Figure 2. Note the similar way in which the corresponding regions evolve in both the simulations and the experimental data. This suggests that at early times during the experiments, the local curvature is a strong driving force in disclination loop evolution.

In long time experiments, other factors enter the picture which make full comparison of simulation to experiment

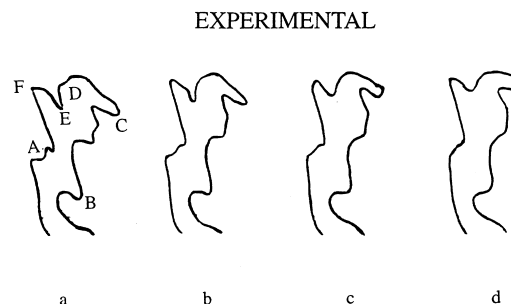


Figure 4 (a) Experimental evolution of the original disclination loop in DHMS-7,9. (a)–(d) A series of tracings taken from light micrographs of the disclination loop during shear relaxation at early times. Loop contours were imaged at 30 s time intervals. The labels ‘A’ to ‘F’ correspond to the same regions as the respective labels in Figure 2

problematic. This is best demonstrated by Figure 5 which shows the continued loop evolution of Figure 4. There is a time interval of 30 s between each tracing in Figure 4 and Figure 5 as well as all subsequent tracings. Over time, there is continued evolution of the ‘nose’ shaped region (indicated as region C in the figure) but this is accompanied by loop elongation in the vertical direction due to the onset of an uncontrolled flow of the material. This distorts the loop and turns the nose region vertical and brings the sides of the nose loop close together. Eventually this enables the loop–loop interaction forces to induce a pinch-off event (Figure 5l–p). The introduction of other forces, such as loop interaction, during late times of the experiment lead to deviations between the theory and the data. However, curvature driven loop motion is very evident just after the pinch-off event occurs. A sharp cusp is left on the original loop just after pinch-off (Figure 5n). This evolves very rapidly and becomes much smoother within just 60 s (Figure 5p). A similar effect is seen in the evolution of the tiny loop shed during the pinch-off event. This also evolved rapidly as a

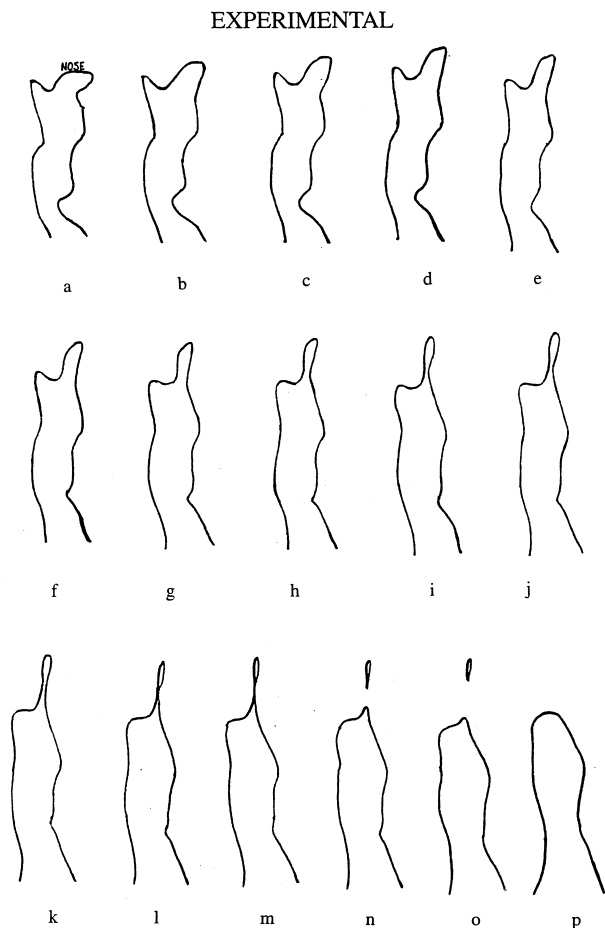


Figure 5 (a)–(p) An experimental series of tracings showing continued evolution of the disclination loop shown in *Figure 4*. The ‘nose’ shaped region indicated in the tracings continues to evolve, but eventually turns upward and becomes elongated due to uncontrolled flow of the material. As the sides of the loop are brought closer together, disclination–disclination interaction forces induce a pinch-off event (30 s time interval between all images)

result of the high curvatures present on the ends of the elliptical shaped loop (*Figure 5n–p*).

The difference between the data and the simulations can also be quantified by means of contour length calculations. The simulations from *Figure 2* and the data from *Figure 4* were used to produce a plot of contour length of a disclination in DHMS-7,9 as a function of time. The results of these calculations are shown in *Figure 6*. The data is shown in reduced form, with CL/CL_0 corresponding to contour length/initial contour length and t/t_{tot} indicating the current interval divided by the total time over which the observations were made. The theoretical contour length decreases monotonically over the entire series of simulations. The experimental data also show an initial rapid decrease but then levels off at $t/t_0 \cong 0.3$ due to contour creation from the onset of flow.

Curvature measurement on disclinations in the liquid crystals 8CB and DHMS-7,9

A series of images of an evolving loop in the liquid crystal 8CB were digitized and compiled into a single plot that is shown in *Figure 7*. The time between each image is about 1 s. The first two images clearly indicate that the high curvature regions evolve much more rapidly than the low curvature regions. Note some lateral shifting between images has occurred due to material flow. At a curvature

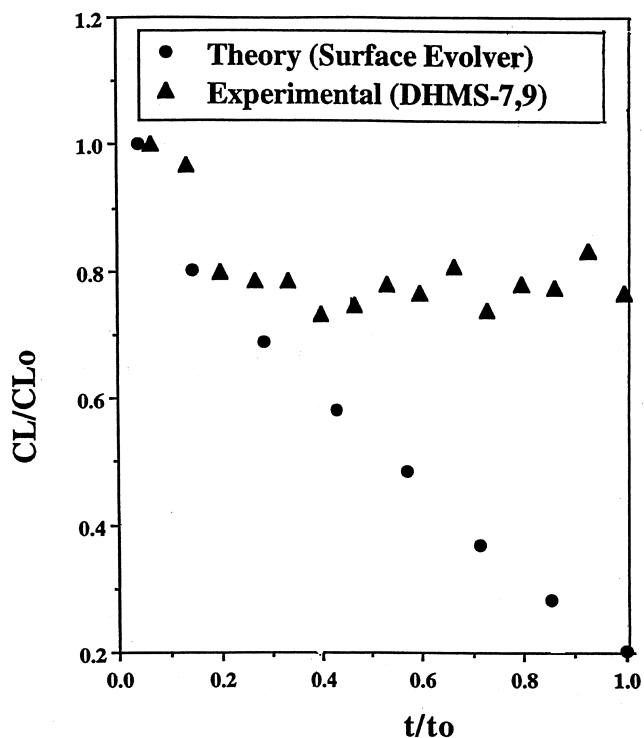


Figure 6 A plot of normalized contour length as a function of time for both simulation and experimental data on DHMS-7,9. The results are shown in reduced form, with CL/CL_0 corresponding to contour length/initial contour length and t/t_{tot} indicating the current time interval divided by the total time over which the observations were made



Figure 7 Schematics of a loop relaxation process in 8CB. The data was digitized with NIH-Image. The time interval between each image is 1 s. Some lateral shift can be seen. However, it is clear that the regions of high curvature (*i.e.* the ends of the ellipses) are evolving more rapidly than the regions of low curvature

of $0.5 \mu\text{m}^{-1}$ the velocity is approximately $9 \mu\text{m/s}$ while at very low curvatures ($10^{-3} \mu\text{m}^{-1}$) the velocity is much lower (approximately $1 \mu\text{m/s}$).

An example of data analysis for the more complex disclination loops observed in DHMS-7,9 is shown as a series of digitized curves made from the data of *Figure 4*. The results are shown in *Figure 8a*. It should be noted that the curves are from data taken at a constant time interval. When the curves are shifted laterally and rotated slightly (*Figure 8b*) they become reasonably superimposed to eliminate a slight amount of relative motion due to some material flow. The high curvature regions in the disclination

contour gradually become smoother. It can also be clearly seen that the individual segments of the curve are moving towards their centers of curvature. The decreased separation distance between the curves as a function of time also shows that the velocity decreases as the curvature becomes smaller.

A plot of velocity *versus* curvature for both 8CB and DHMS-7,9 is shown in Figure 9. The measured velocities are much lower for a given curvature in the polymer than in the 8CB system. This is a result of the different viscosities of the materials. While DHMS-7,9 is studied at a much higher temperature, its viscosity is also much higher than is the

viscosity of 8CB which means that drag forces should impede the motion of disclination loops in the former much more than they would for the latter. In the case of 8CB, where lateral shift was less problematic, it was easier to obtain data over a larger range in curvature which suggests that the velocity *versus* curvature appears to follow a power law. The most interesting feature is the levelling-off of the velocity that occurs in the high curvature region. Apparently, at relatively high curvatures, the disclination motion becomes limited by factor(s) other than just drag forces.

The nature of the disclination core and its relationship to mobility in thermotropic polymers has been addressed by Mazelet and Kleman²⁴. They found that $s = +\frac{1}{2}$ disclinations were 'practically immobile' against soft blows of air on the sample while the $s = -\frac{1}{2}$ defects moved much more readily. They attributed the difference in mobility to a chain end segregation effect. The molecular configuration around an $s = +\frac{1}{2}$ defect core is believed to contain a larger number of chain ends. These must move along with the defect core which greatly reduces the mobility of the $s = +\frac{1}{2}$ defect. The $s = -\frac{1}{2}$ defects on the other hand are much more mobile because chain end segregation can be avoided. The elastic energy of this defect can be minimized by having a vertical director region within the core and some angular regions outside the core. A further discussion on this subject can be found in the book by Donald and Windle²⁵. Dynamics of disclinations in a low molar mass liquid crystal have been addressed by Cladis *et al.*²⁶. It was observed that an $s = -\frac{1}{2}$ disclination core drags surrounding material with it as it moves in order to reduce director rotations.

It is also interesting to note that disclination loops in DHMS-7,9 have consistently more complex shapes than those in low molar mass 8CB. The polymeric LC almost always contains loop structures that each have several regions with wave-like oscillations along the contour of the

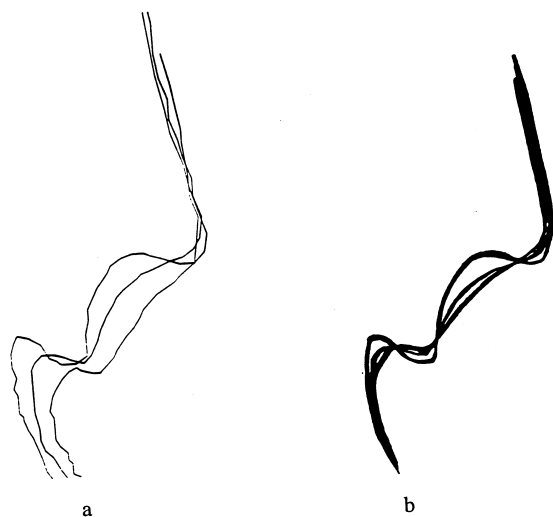


Figure 8 (a) A series of digitized loop contours for the polymer DHMS-7,9. There is a 30 s time interval between each image. Some lateral shift is evident. This data was digitized from Figure 4. (b) The curves overlay when shifted and rotated

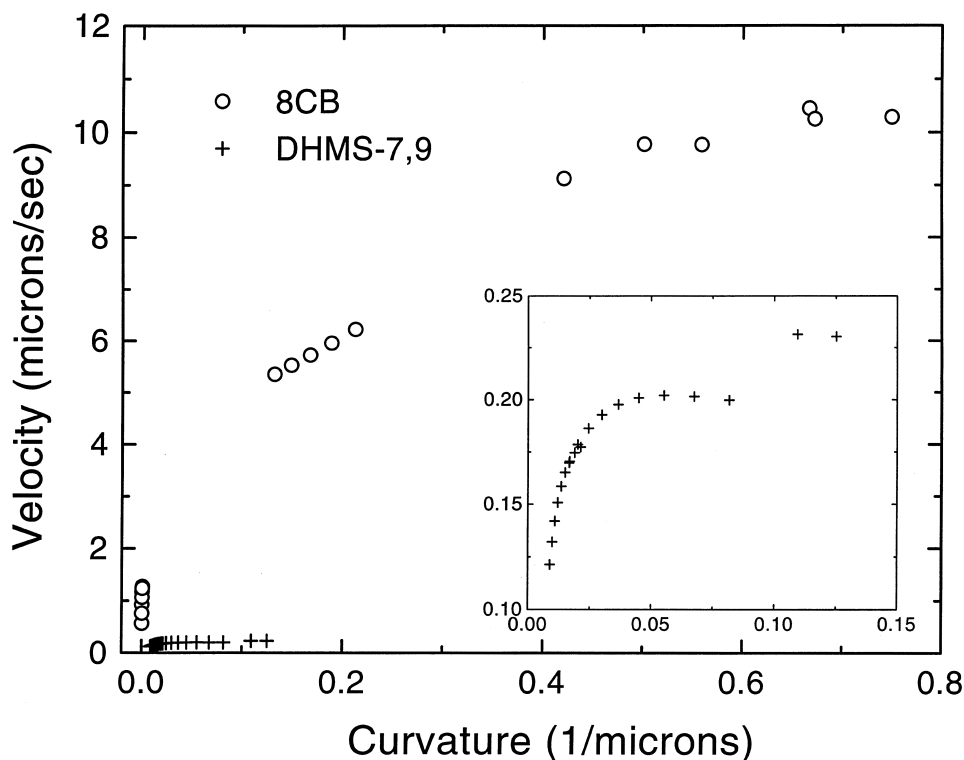


Figure 9 A plot of velocity *versus* curvature for both 8CB and DHMS-7,9. The measured velocities are much lower for a given curvature in the polymer than for the 8CB system

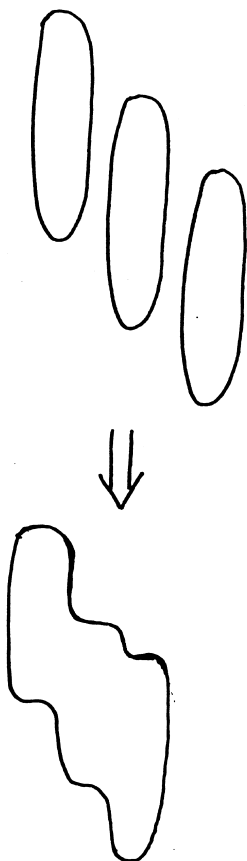


Figure 10 A schematic depicting how loop-loop coalescence could lead to the formation of a new disclination loop with many high curvature regions along its contour

loop. Such features were never seen in 8CB. The high defect density in DHMS-7,9 makes it very likely that many coalescence events are taking place during the shear and subsequent relaxation. Also, the fact that the viscosity is higher for the polymer than it is for the low molar mass LC allows experimental observation of complex contours which would evolve very rapidly in 8CB[†]. A schematic model for the possible origin of complex loop structures is shown in *Figure 10*, wherein three simple loops coalesce and evolve to produce a structure with a complex loop contour.

CONCLUSIONS

The shape evolution of disclination loops after cessation of shear in a low molar mass liquid crystal (8CB) and in a polymeric liquid crystal (DHMS-7,9) were studied using videomicroscopy and a special heating/shearing stage. An algorithm was used to simulate loop motion due to line tension. A local segment moves in a direction along the normal proportional to the curvature, making the relationship of velocity linear with curvature. Digitized sequential images were used to determine the local velocity of the

disclination loops as a function of the local curvature. The disclination line velocity of 8CB was approximately twenty times greater than DHMS-7,9 at a given curvature. Both liquid crystalline materials exhibited a significant departure from a linear relationship of velocity *versus* curvature. The rate of increase of velocity with curvature decreases suggesting that at high curvatures, the motion of the line defect becomes limited by additional drag forces which may arise due to the need for material to diffuse along with the defect core.

ACKNOWLEDGEMENTS

This work was supported by the AFOSR MURI grant #PC218971. J. Gunther would like to thank the AFOSR for a graduate fellowship and Professor S. Allen for helpful discussions. S. Clingman and C. K. Ober would like to thank the Cornell University Materials Science Center.

REFERENCES

1. Carel, R., Thompson, C.V. and Frost, H. J., *Acta Mater.*, 1996, **44**(6), 2479.
2. Sethian, J.A., *Level Set Methods: Evolving Interfaces in Geometry, Fluid mechanics, Computer Vision and Materials Science*. Cambridge University Press, Cambridge, 1996.
3. Chorin, A. J., *Computat. Phys.*, 1985, **57**, 472.
4. Langer, J. S., *Rev. Mod. Phys.*, 1980, **52**, 1.
5. Langer, J. S. and Muller-Krumhaar, H., *Phys. Rev. A*, 1983, **27**, 499.
6. Harker, D. and Parker, E. R., *Trans. Amer. Soc. Metals*, 1945, **34**, 156.
7. Smith, C. S., *Trans. Amer. Inst. of Mining and Metal Eng.*, 1948, **175**, 15.
8. Burke, J. E., *Trans. Amer. Inst. of Mining and Metal Eng.*, 1949, **180**, 73.
9. deGennes, P.G., *The Physics of Liquid Crystals*. Clarendon Press, Oxford, 1975.
10. Pindak, R., Young, C. Y., Meyer, R. B. and Clark, N. A., *Phys. Rev. Lett.*, 1980, **45**, 1193.
11. Chuang, I., Yurke, B., Pargellis, A. N. and Joruk, N., *Phys. Rev. E.*, 1993, **47**, 3343.
12. Grayson, M., *J. Diff. Geom.*, 1987, **26**, 285.
13. Ding, D.-K., Ph.D. Thesis, Massachusetts Institute of Technology, 1994.
14. Graziano, D. J. and Mackley, M. R., *Mol. Cryst. Liq. Cryst.*, 1984, **106**, 103.
15. Graziano, D. J. and Mackley, M. R., *Mol. Cryst. Liq. Cryst.*, 1984, **106**, 73.
16. Nicholson, T. M., Mackley, M. R., Windle, A. H. and Gervat, L., *Phil Trans. Roy. Soc. Lond. A*, 1994, **443**, 1.
17. Mather, P. T., Pearson, D. S. and Larson, R. G., *Liquid Crystals*, 1996, **20**, 539.
18. Starks, C.M., *Phase Transfer Catalysis*. American Chemical Society, Washington, DC, 1987.
19. Hall, E., Ober, C. K., Kramer, E. J., Colby, R. H. and Gillmor, J. R., *Macromolecules*, 1993, **26**, 3764.
20. *CCS 450 Shear Cell Operating Manual*.
21. Osher, R. and Sethian, J. A., *J. Computat. Phys.*, 1988, **79**, 12.
22. Brakke, K. A., *The Surface Evolver Manual*, 1994. See: <http://www.geom.umn.edu/software/evolver/>.
23. Rondeau, K., B.S. Thesis, Massachusetts Institute of Technology, 1996; in addition to private communication with Professor S. Allen.
24. Mazelet, G. and Kleman, M., *Polymer*, 1986, **27**, 714.
25. Donald, A. M. and Windle, A. H., *Liquid Crystalline Polymers*. Cambridge University Press, Cambridge, 1992.
26. Cladis, P. E., van Saarloos, W., Finn, P. L. and Kortan, A. R., *Phys. Rev. Lett.*, 1987, **58**, 222.

[†] ¹¹ shows complex loop shapes done in the low molar mass liquid crystal 5CB immediately after a high density of disclination defects were created via a pressure induced isotropic to nematic transition.